INSTITUTE OF PHYSICS PUBLISHING INVERSE PROBLEMS

Inverse Problems **21** (2005) 1179–1192 doi:10.1088/0266-5611/21/3/023

FBP algorithms for attenuated fan-beam projections

Jiangsheng You[1,2], **Gengsheng L Zeng**[3] **and Zhengrong Liang**[1]

[1] Department of Radiology, State University of New York, Stony Brook, NY 11794, USA
[2] Viisage Technology Inc, 296 Concord Road, 3rd Floor, Billerica, MA 01821, USA
[3] Department of Radiology, University of Utah, Salt Lake City, UT 84108, USA

E-mail: jshyou@mil.sunysb.edu or jyou@viisage.com, larry@ucair.med.utah.edu and jzl@mil.sunysb.edu

Received 7 October 2004, in final form 21 April 2005
Published 13 May 2005
Online at stacks.iop.org/IP/21/1179

Abstract

A filtered backprojection (FBP) reconstruction algorithm for attenuated fan-beam projections has been derived based on Novikov's inversion formula. The derivation uses a common transformation between parallel-beam and fan-beam coordinates. The filtering is shift-invariant. Numerical evaluation of the FBP algorithm is presented. As a special application, we also present a shift-invariant FBP algorithm for fan-beam data reconstruction with uniform attenuation compensation. Several other fan-beam data reconstruction algorithms are discussed. In the attenuation-free case, our algorithm reduces to the conventional fan-beam FBP algorithm.

1. Introduction

Filtered backprojection (FBP) reconstruction algorithms for parallel-beam projection data with and without attenuation have been well established in [1–6]. Without attenuation, the FBP algorithm has been extended to fan-beam data acquisition geometry in [7, 8], and has been widely used in computed tomography (CT). In single photon emission computed tomography (SPECT), the attenuation needs to be compensated for in quantitative studies. However, the existence of an FBP-type algorithm for attenuated fan-beam projections had been an open problem for a while. In [9], the authors presented a circular harmonic decomposition (CHD) reconstruction algorithm for SPECT with fan-beam collimation and uniform attenuation compensation. The CHD method does not indicate any knowledge about the existence of an FBP algorithm for attenuated fan-beam projections. Recently, an explicit inversion formula of FBP type was obtained for attenuated fan-beam projections in [10], but the derivation seemed to be quite complicated to people in the area of engineering and computer science. In this paper, based on Novikov's inversion formula and a partial derivative relation between Cartesian and polar coordinates, an FBP reconstruction algorithm for attenuated fan-beam projections is obtained. The proof seems to be quite elementary compared with other existing work.

The algorithm can be reduced to the special case of uniform attenuation since Novikov's inversion formula is valid when the attenuation map is constant in a unit disc [5] or is zero.

This paper is organized as follows. Section 2 reviews Novikov's inversion formula for parallel-beam geometry. Section 3 describes the derivation of a fan-beam FBP reconstruction algorithm that compensates for non-uniform attenuation. Discretization of the FBP algorithm and computer simulations are presented in section 4. Section 5 concludes the paper with discussions and comments.

2. Review of the FBP expression of Novikov's inversion formula

Let R^2 denote the two-dimensional (2D) Euclidean space with point representation (x, y) or $\vec{r}$ in Cartesian coordinates and (r, φ) in polar coordinates, respectively. For each function $f(x, y)$ in R^2, $f_\theta(s, t) = f(s\cos\theta - t\sin\theta, s\sin\theta + t\cos\theta)$ denotes the same function in Cartesian coordinates $(s, t)_\theta$ that is the rotation of (x, y) by an angle θ along the counter-clockwise direction. The relation between these two coordinates can be depicted by the following transformations:

$$\begin{pmatrix} s \\ t \end{pmatrix} = \begin{pmatrix} \cos\theta & \sin\theta \\ -\sin\theta & \cos\theta \end{pmatrix} \begin{pmatrix} x \\ y \end{pmatrix} \qquad \text{and} \qquad \begin{pmatrix} x \\ y \end{pmatrix} = \begin{pmatrix} \cos\theta & -\sin\theta \\ \sin\theta & \cos\theta \end{pmatrix} \begin{pmatrix} s \\ t \end{pmatrix}. \tag{1}$$

The coordinate (x, y) is defined in the object space, while the coordinate $(s, t)_\theta$ is associated with the rotating detector. Hereafter, we call (x, y) the object coordinate, $(s, t)_\theta$ the parallel-beam detector coordinate and (s, θ) the parallel-beam projection coordinate. For simplicity, we introduce two vector symbols

$$\vec{j} = (\cos\theta, \sin\theta) \qquad \text{and} \qquad \vec{k} = (-\sin\theta, \cos\theta) \tag{2}$$

and one complex symbol $\mathrm{i} = \sqrt{-1}$.

In SPECT imaging, $f(x, y)$ represents the distribution of radiotracer concentration inside the body. The γ-ray photons, emitted from the radiotracer, are attenuated inside the body by a linear attenuation coefficient distribution $\mu(x, y)$ before they arrive at the detector. Let $p(s, \theta)$ be the accumulated photon counts at position s and detector view angle θ in the parallel-beam geometry, then

$$p(s, \theta) = \int_{-\infty}^{\infty} f_\theta(s, t)\, \mathrm{e}^{-a_\theta(s,t)}\, \mathrm{d}t, \tag{3}$$

where $a_\theta(s, t) = \int_t^\infty \mu_\theta(s, \tau)\, \mathrm{d}\tau$. Function $p(s, \theta)$ is the so-called attenuated Radon transform, and will be denoted by $\mathbf{R}_\mu f$. It is known that $f(x, y)$ can be exactly reconstructed from $p(s, \theta)$ using Novikov's inversion formula in parallel-beam geometry. Before presenting that formula, we introduce some mathematical definitions below. Define the Hilbert transform as

$$[\mathbf{H}g](s) = \frac{1}{\pi}\mathrm{pv}\int_{-\infty}^{\infty} \frac{g(l)}{s - l}\, \mathrm{d}l, \tag{4}$$

the Radon transform as

$$[\mathbf{R}f](s, \theta) = \int_{-\infty}^{\infty} f_\theta(s, t)\, \mathrm{d}t, \tag{5}$$

and the derivative of the Hilbert transform as

$$[\mathbf{T}g](s) = \frac{1}{\pi}\mathrm{pv}\int_{-\infty}^{\infty} \frac{g'(l)}{s - l}\, \mathrm{d}l. \tag{6}$$

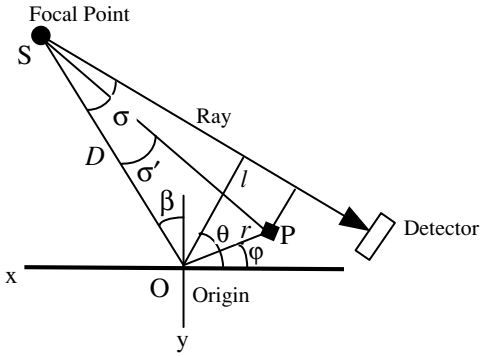

Figure 1. Each projection ray is uniquely determined by (σ, β). Points O and S are the origin and one fan focal point, respectively. P is any point on which the density of radiotracer needs to be reconstructed. Here σ denotes the angle between OS and the projection ray, σ' denotes the angle between OS and PS, β denotes the angle between OS and the y-axis, and D is the distance between the focal point and the origin.

Using the conventions of [4], Novikov's inversion formula can be expressed as

$$\begin{aligned} f(x,y) &= \mathrm{Re}\,\frac{1}{4\pi}\int_0^{2\pi}\frac{\partial}{\partial s}(\mathrm{e}^{a_\theta(s,t)-h(s,\theta)}[\mathbf{H}\,\mathrm{e}^{h}p](s,\theta))\,\mathrm{d}\theta \\ &= \mathrm{Re}\,\frac{1}{4\pi}\int_0^{2\pi}(\mathrm{e}^{a_\theta(s,t)-h(s,\theta)}[\mathbf{T}\,\mathrm{e}^{h}p](s,\theta)+\frac{\partial}{\partial s}\,\mathrm{e}^{a_\theta(s,t)-h(s,\theta)}[\mathbf{H}\,\mathrm{e}^{h}p](s,\theta))\,\mathrm{d}\theta \\ &= \mathrm{Re}\,\frac{1}{4\pi}\left[\int_0^{2\pi}\int_{-\infty}^{\infty}\frac{\mathrm{e}^{a_\theta(s,t)-h(s,\theta)}}{\pi(s-l)}\frac{\partial}{\partial l}(\mathrm{e}^{h}p)(l,\theta)\,\mathrm{d}l\,\mathrm{d}\theta\right. \\ &\quad \left.+\int_0^{2\pi}\int_{-\infty}^{\infty}\frac{\partial}{\partial s}\,\mathrm{e}^{a_\theta(s,t)-h(s,\theta)}\frac{(\mathrm{e}^{h}p)(s,\theta)}{\pi(s-l)}\,\mathrm{d}l\,\mathrm{d}\theta\right], \end{aligned} \tag{7}$$

where $s = x\cos\theta + y\sin\theta$, $t = -x\sin\theta + y\cos\theta$, $h(s,\theta) = \frac{1}{2}[(\mathbf{R} + \mathrm{i}\mathbf{H}\mathbf{R})\mu](s,\theta)$ and l indicates the rays in the parallel-beam geometry. Equation (7) is originally understood as two ordered one-dimensional (1D) integrals with respect to l and θ [3, 4]. If $f(x,y)$ and $\mu(x,y)$ are smooth, (7) is also valid in the sense of a 2D integral with respect to (l,θ). With Fubini's theorem, there would be no difference between the two ordered 1D integrals and the 2D integral, so that we are able to perform the 2D coordinate transformation and to exchange the order of the 1D integrals in (7) with respect to l and θ. The detailed derivation of (7) can be found in [3, 4]. Note that (7) is slightly different from its original form in [3, 4]. The reason that we use the operators **T** and **H** is to emphasize the procedure of a classical FBP-type reconstruction. The attenuation map $\mu(x,y)$ is assumed to be known in this paper, thus $a_\theta(s,t)$ and $h(s,\theta)$ should be available in any coordinates because they can be calculated in advance.

3. Derivation of an FBP algorithm for fan-beam projections

Assume that the focal point positions are distributed on a circle with its centre at the origin. One view of the fan-beam data acquisition geometry is described in figure 1.

First, we introduce two notations of (σ,β) which will be called fan-beam projection coordinate and $(\rho,\sigma)_\beta$ which denotes the polar coordinate with the origin at S. Compared

with the parallel-beam geometry, (σ, β) corresponds to (l, θ) by the following relations:

$$l = D\sin\sigma, \qquad \theta = \sigma + \beta. \tag{8}$$

The Jacobian of the transformation from (σ, β) to (l, θ) is $D\cos\sigma$, which is always positive for $-\pi/2 < \sigma < \pi/2$. If the support of $f(x, y)$ and $\mu(x, y)$ is in a disc with radius less than D, the mapping between (σ, β) to (l, θ) is one-to-one inside that disc. Also, we have the following geometric relation,

$$r\cos(\theta - \varphi) - l = K\sin(\sigma' - \sigma), \tag{9}$$

where

$$K = \sqrt{r^2 + D^2 + 2rD\sin(\beta - \varphi)} \tag{10}$$

and

$$K\sin\sigma' = r\cos(\beta - \varphi). \tag{11}$$

The detailed derivation of (9) can be found, for example, in [7, 8] by considering a simple triangular geometry. Define the weighted fan-beam projection $g(\sigma, \beta)$ as

$$g(\sigma, \beta) = (\mathrm{e}^h p)(D\sin\sigma, \sigma + \beta) \tag{12}$$

for the fan-beam geometry. Assume that $f(x, y)$ and $\mu(x, y)$ are smooth, then we have

$$D\cos\sigma\frac{\partial}{\partial\sigma}g(\sigma, \beta) = \frac{\partial}{\partial l}(\mathrm{e}^h p)(l, \theta)|_{l=D\sin\sigma, \theta=\sigma+\beta}. \tag{13}$$

Equation (13) seems to be observed for the first time, and turns out to be the key relation to derive an FBP algorithm for fan-beam data. For each focal point position β and a fixed point (x, y), the weighting factor $\mathrm{e}^{a_\theta(s,t)-h(s,\theta)}$ is a function of the line PS. From figure 1, the representation of PS with the coordinate of (l, θ) is $(r\cos(\beta - \varphi), \sigma' + \beta)$. Thus, in the fan-beam coordinate system (σ, β), the weighting factors in (7) can be expressed as follows,

$$W_\beta(r, \varphi, \sigma') = \mathrm{e}^{a_\theta(s,t)-h(s,\theta)}|_{\theta=\sigma'+\beta, s=r\cos(\theta-\varphi), t=r\sin(\theta-\varphi)}, \tag{14}$$

$$W^1_\beta(r, \varphi, \sigma') = \left.\frac{\partial\,\mathrm{e}^{a_\theta(s,t)-h(s,\theta)}}{\partial s}\right|_{\theta=\sigma'+\beta, s=r\cos(\theta-\varphi), t=r\sin(\theta-\varphi)}. \tag{15}$$

Now, we rewrite the two terms of (7) as follows,

$$\begin{aligned}
&\int_0^{2\pi}\int_{-\infty}^{\infty}\frac{\mathrm{e}^{a_\theta(s,t)-h(s,\theta)}}{\pi(s-l)}\frac{\partial}{\partial l}(\mathrm{e}^h p)(l, \theta)\,\mathrm{d}l\,\mathrm{d}\theta \\
&\quad= \int_0^{2\pi}\int_{-\pi/2}^{\pi/2}\frac{W_\beta(r, \varphi, \sigma')(D\cos\sigma)^2}{\pi K\sin(\sigma' - \sigma)}\frac{\partial g(\sigma, \beta)}{\partial\sigma}\,\mathrm{d}\sigma\,\mathrm{d}\beta \\
&\quad= \int_0^{2\pi}\frac{W_\beta(r, \varphi, \sigma')}{\pi K}\,\mathrm{d}\beta\int_{-\pi/2}^{\pi/2}\frac{D^2\cos^2\sigma}{\sin(\sigma' - \sigma)}\frac{\partial g(\sigma, \beta)}{\partial\sigma}\,\mathrm{d}\sigma
\end{aligned} \tag{16}$$

and

$$\begin{aligned}
&\int_0^{2\pi}\int_{-\infty}^{\infty}\frac{\partial}{\partial s}\mathrm{e}^{a_\theta(s,t)-h(s,\theta)}\frac{(\mathrm{e}^h p)(s, \theta)}{\pi(s-l)}\,\mathrm{d}l\,\mathrm{d}\theta \\
&\quad= \int_0^{2\pi}\int_{-\pi/2}^{\pi/2}W^1_\beta(r, \varphi, \sigma')\frac{g(\sigma, \beta)D\cos\sigma}{\pi K\sin(\sigma' - \sigma)}\,\mathrm{d}\sigma\,\mathrm{d}\beta \\
&\quad= \int_0^{2\pi}\frac{W^1_\beta(r, \varphi, \sigma')}{\pi K}\,\mathrm{d}\beta\int_{-\pi/2}^{\pi/2}\frac{g(\sigma, \beta)D\cos\sigma}{\sin(\sigma' - \sigma)}\,\mathrm{d}\sigma,
\end{aligned} \tag{17}$$

where

$$\sigma' = \arcsin\left(\frac{r\cos(\beta-\varphi)}{K}\right). \tag{18}$$

Apparently, both (16) and (17) follow the typical FBP procedure for the weighted fan-beam projections $g(\sigma, \beta)$, thus an FBP reconstruction algorithm has been derived for attenuated fan-beam projections via Novikov's inversion formula. Since both **T** and **H** are shift-invariant, they can be replaced by any other regularized kernel functions without changing the reconstruction procedure of an FBP-type. The calculations are based on the angular expression (σ, β) of the projection ray, and can be extended to any other coordinate expression $(\eta(\sigma), \beta)$ if $\eta(\sigma)$ is a one-to-one mapping, e.g., equally spaced sampling along the detector.

Note that $g(\sigma, \beta)$ in our formula is the weighted fan-beam projection, instead of the attenuated Radon transform, and the attenuated projection has to be weighted by a complex function $e^{h(s,\theta)}$ before using our algorithm. Define the angular Hilbert transform, similar to [10], as

$$[\mathbf{\Gamma} g](\sigma) = \frac{1}{\pi}\mathrm{pv}\int_{-\pi/2}^{\pi/2}\frac{g(\gamma)}{\sin(\sigma-\gamma)}\,\mathrm{d}\gamma. \tag{19}$$

It has been known in [11] that the term $[\mathbf{HR}\mu](l, \theta)$ in $h(s, \theta)$ can be evaluated by the angular Hilbert transform of fan-beam projections. Actually, we have the following equation,

$$[\mathbf{\Gamma} k](\sigma, \beta) = [\mathbf{HR}\mu](D\sin\sigma, \sigma+\beta), \tag{20}$$

where $k(\sigma, \beta) = [\mathbf{R}\mu](D\sin\sigma, \sigma+\beta)$ is the fan-beam projection of $\mu(x, y)$, and the angular Hilbert transform $\mathbf{\Gamma}$ is performed on the first variable of $k(\sigma, \beta)$. A derivation of (20) can be found in appendix A. Therefore the weighted fan-beam projection $g(\sigma, \beta)$ can be calculated using $k(\sigma, \beta)$ without extra interpolations between parallel-beam and fan-beam projection coordinates, i.e., we use the following formula:

$$g(\sigma, \beta) = e^{\frac{1}{2}[(\mathbf{I}+\mathrm{i}\mathbf{\Gamma})k](\sigma,\beta)}\,p(D\sin\sigma, \sigma+\beta). \tag{21}$$

To summarize, the image f can be reconstructed by the following FBP-type formula,

$$\begin{aligned} f(r,\varphi) = {} & \frac{1}{4\pi}\mathrm{Re}\int_0^{2\pi}\frac{W_\beta(r,\varphi,\sigma')}{\pi K}\,\mathrm{d}\beta\int_{-\pi/2}^{\pi/2}\frac{D^2\cos^2\sigma}{\sin(\sigma'-\sigma)}\frac{\partial g(\sigma,\beta)}{\partial\sigma}\,\mathrm{d}\sigma \\ & + \frac{1}{4\pi}\mathrm{Re}\int_0^{2\pi}\frac{W_\beta^1(r,\varphi,\sigma')}{\pi K}\,\mathrm{d}\beta\int_{-\pi/2}^{\pi/2}\frac{g(\sigma,\beta)D\cos\sigma}{\sin(\sigma'-\sigma)}\,\mathrm{d}\sigma, \end{aligned} \tag{22}$$

where K and σ' are defined by (10) and (18), respectively. The attenuation map $\mu(x, y)$ and the reconstructed image are commonly expressed in the Cartesian coordinates. Also, it has been observed that the image reconstruction is not very sensitive to the noise in the attenuation map [6]. For simplicity of implementation, we would rather evaluate $a_\theta(s, t)$ in the detector coordinate system $(s, t)_\theta$ even it could be expressed in the fan-beam projection coordinate (σ, β).

4. Computer simulation

Equation (22) is an exact reconstruction formula that contains explicit differential operation. Like the Shepp–Logan filter in the classical FBP algorithm for parallel-beam projections [1], we use a regularized version of the operator **T** so that the explicit differential operation can be carried out by linear convolution. Hereafter, $T(l)$ will stand for the regularized kernel function of **T**, and $H(l)$ will stand for the kernel function of the Hilbert transform. More

properties of $H(l)$ and $T(l)$ can be found in appendix B. By using $H(l)$ and $T(l)$ in (7), with relations (8)–(12), we have the following reconstruction formula:

$$f(r,\varphi) \approx \frac{1}{4\pi}\mathrm{Re}\int_0^{2\pi} W_\beta(r,\varphi,\sigma')\,\mathrm{d}\beta \int_{-\pi/2}^{\pi/2} T(K\sin(\sigma'-\sigma))D\cos\sigma\, g(\sigma,\beta)\,\mathrm{d}\sigma + \frac{1}{4\pi}\mathrm{Re}\int_0^{2\pi} W_\beta^1(r,\varphi,\sigma')\,\mathrm{d}\beta \int_{-\pi/2}^{\pi/2} H(K\sin(\sigma'-\sigma))D\cos\sigma\, g(\sigma,\beta)\,\mathrm{d}\sigma. \tag{23}$$

Note that the approximation is due to the fact that $T(l)$ is the regularized kernel for the operator $\mathbf{T}$.

It can be seen that the major computations come from the weighting factors $W_\beta(r,\varphi,\sigma')$ and $W_\beta^1(r,\varphi,\sigma')$, which require the evaluation of attenuation-related functions $a_\theta(s,t)$ and $h(s,\theta)$. Since the attenuation map $\mu(x,y)$ is usually expressed in the Cartesian coordinates (x,y), in the evaluation of $a_\theta(s,t)$, $\mu_\theta(s,t)$ was then calculated through the coordinate transformation between (x,y) and $(s,t)_\theta$, which involved bilinear interpolations. On the other hand, in the evaluation of $h(s,\theta)$ for calculating $g(\sigma,\beta)$, the fan-beam projection $k(\sigma,\beta)$ of $\mu(x,y)$ was calculated through the coordinate transformation from (x,y) to $(\rho,\sigma)_\beta$. Because only the real part is needed in the final reconstruction, we do not evaluate the terms that contribute to the imaginary part in (23). In summary, the attenuated fan-beam data inversion formula (23) can be realized by the following steps. (i) Pre-calculate the weighting factors $\mathrm{e}^{a_\theta(s,t)-h(s,\theta)}$ and $\mathrm{e}^{\frac{1}{2}[(\mathbf{I}+\mathrm{i}\boldsymbol{\Gamma})k](\sigma,\beta)}$, and multiply $\mathrm{e}^{\frac{1}{2}[(\mathbf{I}+\mathrm{i}\boldsymbol{\Gamma})k](\sigma,\beta)}$ to the acquired fan-beam projection to obtain $g(\sigma,\beta)$. (ii) Evaluate the two convolutions in (23). (iii) Evaluate the weighted fan-beam backprojection with the corresponding weighting functions $W_\beta(r,\varphi,\sigma')$ and $W_\beta^1(r,\varphi,\sigma')$.

4.1. Discretization of reconstruction formula

Next, we need to specify the definitions of $H(K\sin\sigma)$ and $T(K\sin\sigma)$ in (23) for computer simulations. Let δ be the sampling step of angular variable σ in the subsequent simulation, then $T(K\sin\sigma)$ was chosen as the following Shepp–Logan-like filter:

$$\begin{aligned} T(K\sin\sigma) &= \frac{\sigma^2}{2\pi(K\sin\sigma)^2}\int_{-\pi/\delta}^{\pi/\delta}\frac{|2\sin(\delta\omega/2)|}{\delta}\,\mathrm{e}^{\mathrm{i}\sigma\omega}\,\mathrm{d}\omega \\ &= \frac{\sigma^2}{(K\sin\sigma)^2}\mathrm{SL}_\delta(\sigma) \\ &= \frac{1}{K^2}T_{\mathrm{SL}}(\sigma), \end{aligned} \tag{24}$$

where $\mathrm{SL}_\delta(\sigma)$ denotes the Shepp–Logan filter and $T_{\mathrm{SL}}(\sigma) = \mathrm{SL}_\delta(\sigma)\sigma^2/\sin^2\sigma$. The derivation of (24) is given in appendix B. The discrete form of $T_{\mathrm{SL}}(\sigma)$ is expressed as

$$T_{\mathrm{SL}}(n\delta) = \frac{n^2}{\pi(0.25-n^2)\sin^2(n\delta)}, \tag{25}$$

where $n \neq 0$ and $T_{\mathrm{SL}}(0) = 4.0/(\pi\delta^2)$. The kernel $\Gamma(\sigma)$ of the angular Hilbert transform $\boldsymbol{\Gamma}$ takes the following form,

$$\Gamma(\sigma) = \frac{1}{\pi\sin\sigma}, \tag{26}$$

where $\sigma \neq 0$ and $\Gamma(0) = 0$. Using the definition of $H(l)$ as given in appendix B, the function $H(K\sin\sigma)$ is expressed as

$$H(K\sin\sigma) = \Gamma(\sigma)/K. \tag{27}$$

Let f^1 and f^2 be the first and the second terms in (23), respectively. Then

$$f^1(r,\varphi) = \frac{1}{4\pi}\,\mathrm{Re}\int_0^{2\pi} W_\beta(r,\varphi,\sigma')g_F^1(\sigma',\beta)\frac{1}{K^2}\,\mathrm{d}\beta \tag{28.1}$$

and

$$f^2(r,\varphi) = \frac{1}{4\pi}\,\mathrm{Re}\int_0^{2\pi} W_\beta^1(r,\varphi,\sigma')g_F^2(\sigma',\beta)\frac{1}{K}\,\mathrm{d}\beta, \tag{28.2}$$

where

$$g_F^1(\sigma',\beta) = \int_{-\pi/2}^{\pi/2} T_{\mathrm{SL}}(\sigma'-\sigma)D\cos\sigma\, g(\sigma,\beta)\,\mathrm{d}\sigma \tag{29.1}$$

and

$$g_F^2(\sigma',\beta) = \int_{-\pi/2}^{\pi/2} \Gamma(\sigma'-\sigma)D\cos\sigma\, g(\sigma,\beta)\,\mathrm{d}\sigma. \tag{29.2}$$

In computer implementation, parameters were discretized as $\mathrm{d}\sigma = \delta$, $\sigma = n\delta$ and $\sigma' = n'\delta$ in calculating g_F^1 and g_F^2. In calculating f^1 and f^2, $\mathrm{d}\beta = \Omega$ and $\beta_k = k\Omega$. Note that in the backprojection step, a linear interpolation was used for σ'. The discrete counterparts of functions W_β and W_β^1 were A_k and B_k (their definitions are given below), respectively. Now, for a fixed point (x, y), the discretized versions of (28) and (29) can be described as the combination of the filtering step

$$\begin{aligned} g_F^1(n',\beta_k) &= \delta D\sum_n T_{\mathrm{SL}}((n'-n)\delta)\cos(n\delta)g(n\delta,\beta_k)\\ g_F^2(n',\beta_k) &= \delta D\sum_n \Gamma((n'-n)\delta)\cos(n\delta)g(n\delta,\beta_k), \end{aligned} \tag{30.1}$$

and the subsequent backprojection step

$$\begin{aligned} f^1(x,y) &= \frac{\Omega}{4\pi}\,\mathrm{Re}\sum_k A_k\big((1-\lambda_{n'(k)})g_F^1(n'(k),\beta_k) + \lambda_{n'(k)}g_F^1(n'(k)+1,\beta_k)\big)\big/K_k^2\\ f^2(x,y) &= \frac{\Omega}{4\pi}\,\mathrm{Re}\sum_k B_k\big((1-\lambda_{n'(k)})g_F^2(n'(k),\beta_k) + \lambda_{n'(k)}g_F^2(n'(k)+1,\beta_k)\big)\big/K_k, \end{aligned} \tag{30.2}$$

where

$$\begin{aligned} &K_k = \sqrt{x^2+y^2+D^2+2xD\sin\beta_k - 2yD\cos\beta_k},\\ &\sigma_k = \arcsin\left(\frac{x\cos\beta_k + y\sin\beta_k}{K_k}\right),\\ &n'(k) = \mathrm{floor}(\sigma_k/\delta), \qquad \lambda_{n'(k)} = \sigma_k/\delta - n'(k),\\ &s_k = x\cos(\beta_k+\sigma_k) + y\sin(\beta_k+\sigma_k),\\ &t_k = -x\sin(\beta_k+\sigma_k) + y\cos(\beta_k+\sigma_k),\\ &A_k = \exp\big(a_{(\beta_k+\sigma_k)}(s_k,t_k) - h_+(s_k,\beta_k+\sigma_k)\big), \end{aligned}$$

and

$$\begin{aligned} B_k = \big(&\exp\big(a_{(\beta_k+\sigma_k)}(s_k+\Delta,t_k) - h_+(s_k+\Delta,\beta_k+\sigma_k)\big)\\ &-\exp\big(a_{(\beta_k+\sigma_k)}(s_k-\Delta,t_k) - h_+(s_k-\Delta,\beta_k+\sigma_k)\big)\big)\big/(2\Delta), \end{aligned}$$

where Δ is the sampling step of variables s in $(s,t)_\theta$. Also note that the calculations of A_k and B_k may need interpolations since $\mu(x,y)$ is only known on a discrete grid. Combining $f^1(x,y)$ and $f^2(x,y)$, image $f(x,y)$ is reconstructed.

(a) (b) (c)

Figure 2. Phantoms: (a) emission distribution, (b) nonuniform attenuation map, (c) uniform attenuation map.

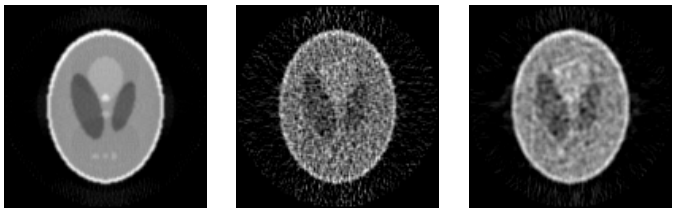

(a) (b) (c)

Figure 3. Reconstructed images: (a) from noise-free data, (b) from noisy data, (c) from filtered noisy data.

4.2. Numerical experiment

Without loss of generality, we assume that both the object function $f(x, y)$ and attenuation map $\mu(x, y)$ are defined in an unit circle. In our computer simulations, the object $f(x, y)$ was chosen as the Shepp–Logan phantom and the attenuation map $\mu(x, y)$ was a modified chest phantom, similar to [5] (see figure 2). $f(x, y)$ and $\mu(x, y)$ were sampled into 128×128 digital images. The Shepp–Logan phantom includes several fine objects and multiple intensity levels so that it can be used to measure how an algorithm affects the reconstruction in terms of spatial resolution and image contrast, see details in [12]. The attenuation map contains three different attenuation levels with linear attenuation coefficients of 0.25, 0.75 and 1.00 in five objects mimicking the lungs, soft tissue and bones, respectively. Also, in order to identify any artefacts that the discontinuity of the emission object and attenuation map might have, the attenuation map was designed to have different structures compared with the Shepp–Logan emission phantom so that the discontinuous edges in the Shepp–Logan phantom and attenuation map are different. In particular, the support region of attenuation map is larger than the support region of emission phantom. This is different from the phantoms used in [4, 5].

The geometric parameters of the fan-beam data acquisition are described as follows. The fan-focal length $D = 2.0$, and the subtending angle was 60° that fully covered the support region of the emission phantom and attenuation map. Both noise-free and noisy projection data were generated with 128 views evenly spaced over 360° on a circular orbit. At each view, there were 128 projection samples with equiangular fan-beam rays. The sampling rate used in this paper seems to be more realistic compared with that in [10]. The image was reconstructed into a 128×128 image array. The reconstructed images are displayed in figure 3 with the negative values set to zero. In all displays, the images were linearly scaled so that the maximal values were scaled to 255. A profile drawn horizontally across the reconstructed image through the centre is shown in figure 4, where the true image values are

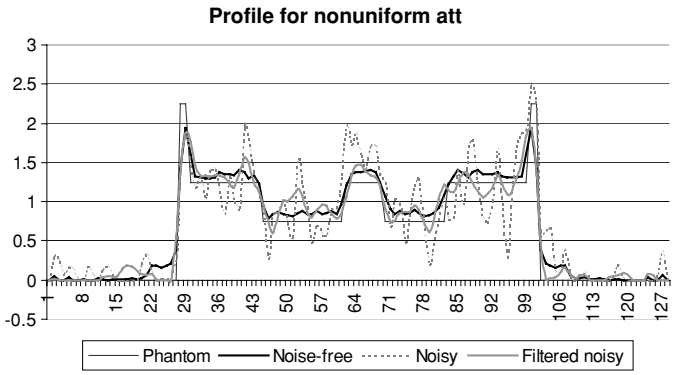

Figure 4. Profiles of the emission phantom and the reconstructed images.

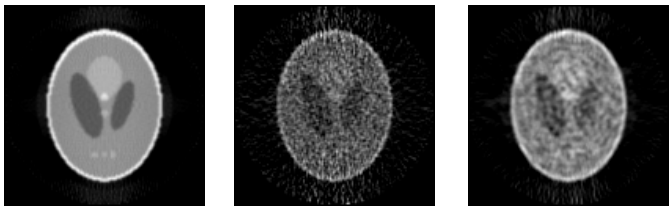

(a) (b) (c)

Figure 5. Reconstructed images: (a) from noise-free data, (b) from noisy data, (c) from filtered noisy data.

shown. As expected, the attenuation has been compensated for in the reconstructed image. For noise analysis, we define the signal-to-noise ratio (SNR) of an observed or estimated image $S(m, n)$ as $\mathrm{SNR}(I, S) = L_2(I)/L_2(I - S)$, here $I(m, n)$ is the true mean image. In the simulation, the noisy projection was generated using the Poisson deviate generator in [13], and the SNR of the noisy projection data was 8.07 with total counts of 641 972. The SNRs of the reconstructed images from noise-free and noisy data are 5.04 and 2.59, respectively. Numerical experiments with noisy projections were reported in [10], but no noise treatment methods were mentioned. In order to filter the noise in the reconstructed images, following the noise treatment method in [6], we used the median filter to estimate the mean of projection $g(\sigma, \beta)$, and the five-point symmetric Savitzky–Golay filter (see details in [13]) to smooth the filtered projection $g_F^1(\sigma, \beta)$ in (29.1). The reconstructed image from filtered noisy projection is shown in figure 3, and the SNR became 3.82. In this simulation, the applied filtering process does improve the SNR. The simple statistic of noisy projection data was derived to suggest optimal filters for parallel-beam projection data in [14], but the analysis might not be directly applied to the fan-beam data due to the irregularity of fan-beam geometry.

We also conducted a simulation study when the attenuation coefficient was a constant value of 0.75 inside the largest ellipse in figure 2. The reconstructed images are shown in figure 5. The profiles drawn horizontally across the phantom and reconstructed images through the centre are shown in figure 6. In the simulation, the SNR of the noisy projection was 7.63 with total counts of 588 055. The SNRs of the reconstructed images from noise-free and noisy data were 4.83 and 2.38, respectively. After applying the median and Savitzky–Golay filters, the SNR of the reconstructed image became 3.60.

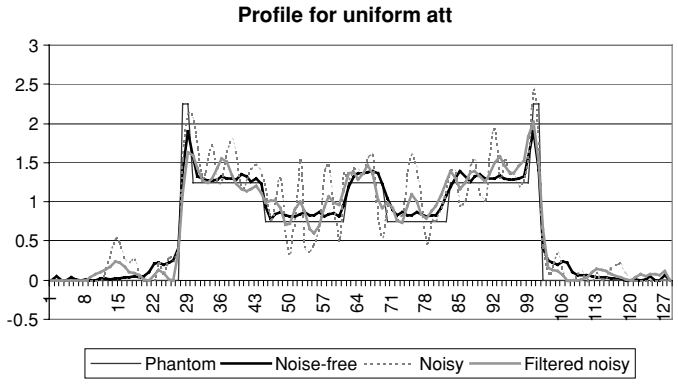

Figure 6. Profiles of the emission phantom and the reconstructed images.

5. Discussion and conclusion

In this paper, we derived an FBP algorithm for attenuated fan-beam SPECT data. The filtering is shift-invariant. Our fan-beam formula looks similar to the conventional fan-beam FBP algorithms [7, 8]. As a special case, we presented a shift-invariant FBP algorithm for fan-beam SPECT reconstruction with uniform attenuation compensation. Since the kernel function in the Tretiak–Metz inversion formula [2] includes an exponential constant so that it is inhomogeneous, as a result, the Tretiak–Metz inversion formula might not directly accommodate an FBP algorithm for uniformly attenuated fan-beam projections. When the attenuation is neglected, i.e., $\mu \equiv 0$, the second term of (23) vanishes and the first term of (23) reduces to the conventional fan-beam FBP algorithm [7, 8]. Computer simulations were provided for both non-uniform attenuation and uniform attenuation inside an ellipse. Similar to the result in [6] for parallel-beam projections, the second term of (23) was also found to have very minor contribution to the reconstruction.

In fact, there are many fan-beam data inversion formulae that can be derived through regularizing the operators **T** and **H** in different ways. For example, $T(K \sin\sigma)$ can be chosen as the following ramp filter,

$$T(K\sin\sigma) = \frac{\sigma^2}{2\pi(K\sin\sigma)^2}\int_{-\pi/\delta}^{\pi/\delta} |\omega|\, \mathrm{e}^{\mathrm{i}\omega\sigma}\, \mathrm{d}\omega \tag{31}$$

or other smoother ones like the Hanning filter, and $H(l)$ can be chosen as the similar kernels used in [4, 5]. More properties of **T** and **H** can be found in appendix B.

A reconstruction formula, similar to [10], can be readily obtained through the following coordinate transformation,

$$\begin{aligned} f(x,y) &= \mathrm{Re}\,\frac{1}{4\pi}\,\mathrm{div}\int_0^{2\pi} \vec{j}\,\mathrm{e}^{a_\theta(s,t)-h(s,\theta)}[\mathbf{H}\,\mathrm{e}^{h}p](s,\theta)\,\mathrm{d}\theta \\ &= \mathrm{Re}\,\frac{1}{4\pi}\,\mathrm{div}\int_0^{2\pi}\int_{-\pi/2}^{\pi/2} \vec{j}\,\mathrm{e}^{a_\theta(s,t)-h(s,\theta)}\frac{\mathrm{e}^{h(l,\theta)}p(l,\theta)}{s-l}\,\mathrm{d}l\,\mathrm{d}\theta \\ &= \mathrm{Re}\,\frac{1}{4\pi}\,\mathrm{div}\int_0^{2\pi}\int_{-\pi/2}^{\pi/2} \vec{A}_\beta(r,\varphi,\sigma')\frac{D\cos\sigma\, g(\sigma,\beta)}{K\sin(\sigma'-\sigma)}\,\mathrm{d}\sigma\,\mathrm{d}\beta \\ &= \mathrm{Re}\,\frac{1}{4\pi}\,\mathrm{div}\int_0^{2\pi}\frac{\vec{A}_\beta(r,\varphi,\sigma')D}{K}\,\mathrm{d}\beta\int_{-\pi/2}^{\pi/2}\frac{\cos\sigma\, g(\sigma,\beta)}{\sin(\sigma'-\sigma)}\,\mathrm{d}\sigma, \end{aligned} \tag{32}$$

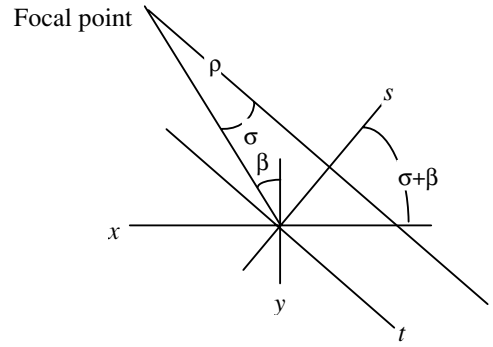

Figure 7. Illustration of coordinates $(\rho, \sigma)_\beta$ and $(s, t)_{\sigma+\beta}$.

where

$$\vec{A}_\beta(r, \varphi, \sigma') = \vec{j}\, \mathrm{e}^{a_\theta(s,t)-h(s,\theta)}|_{\theta=\sigma'+\beta, s=r\cos(\theta-\varphi), t=r\sin(\theta-\varphi)}.$$

In this paper, we considered reconstruction algorithms for equiangular fan-beam detectors. It is straightforward to derive similar results for equally spaced fan-beam detectors (see appendix C).

Acknowledgments

GLZ was supported in part by NIH grants CA100181 and EB00121, and ZL was supported in part by NIH grant HL51466. The authors would like to express their deep thanks to the reviewers for their constructive suggestions.

Appendix A. Proof of equation (20)

Let $\mu_\beta^{\mathrm{pol}}(\rho, \sigma)$ denote the attenuation map in the polar coordinates $(\rho, \sigma)_\beta$, where the relationship between coordinates $(\rho, \sigma)_\beta$ and $(s, t)_{\sigma+\beta}$ is shown in figure 7.

For any σ, we have the following formula,

$$\begin{aligned}
[\mathbf{\Gamma} k](\sigma, \beta) &= \frac{1}{\pi}\mathrm{pv}\int_{-\pi/2}^{\pi/2} \frac{k(\gamma, \beta)}{\sin(\sigma-\gamma)}\,\mathrm{d}\gamma \\
&= \frac{1}{\pi}\mathrm{pv}\int_{-\pi/2}^{\pi/2} \frac{\mathrm{d}\gamma}{\sin(\sigma-\gamma)}\int_0^\infty \mu_\beta^{\mathrm{pol}}(\rho, \gamma)\,\mathrm{d}\rho \\
&= \frac{1}{\pi}\mathrm{pv}\int_{-\pi/2}^{\pi/2}\int_0^\infty \frac{\mu_\beta^{\mathrm{pol}}(\rho, \gamma)}{\sin(\sigma-\gamma)}\,\mathrm{d}\rho\,\mathrm{d}\gamma \\
&= \frac{1}{\pi}\mathrm{pv}\int_{-\pi/2}^{\pi/2}\int_0^\infty \frac{\mu_\beta^{\mathrm{pol}}(\rho, \gamma)}{\rho\sin(\sigma-\gamma)}\rho\,\mathrm{d}\rho\,\mathrm{d}\gamma \\
&= \frac{1}{\pi}\mathrm{pv}\int_{-\infty}^{\infty}\int_{-\infty}^{\infty} \frac{\mu_{\sigma+\beta}(s, t)}{D\sin\sigma - s}\,\mathrm{d}s\,\mathrm{d}t \\
&= [\mathbf{HR}\mu](D\sin\sigma, \sigma+\beta), \qquad \text{(A.1)}
\end{aligned}$$

where the coordinate transformation from $(\rho, \sigma)_\beta$ to $(s, t)_{\sigma+\beta}$ is

$$\begin{pmatrix} s \\ t \end{pmatrix} = \begin{pmatrix} \rho \sin(\gamma - \sigma) + D \sin\sigma \\ \rho \cos(\gamma - \sigma) - D \cos\sigma \end{pmatrix}. \tag{A.2}$$

Thus, equation (20) is derived.

Appendix B. Properties of T and H

Let $T(l)$ and $H(l)$ be the kernel functions of operators **T** and **H**, respectively. In their exact forms, $T(l)$ and $H(l)$ can be understood as the generalized Fourier transforms:

$$T(l) = \frac{1}{2\pi} \int_{-\infty}^{\infty} |\omega| \, \mathrm{e}^{\mathrm{i}\omega l} \, \mathrm{d}\omega, \tag{B.1}$$

$$H(l) = -\frac{1}{2\pi} \int_{-\infty}^{\infty} \mathrm{i} \, \mathrm{sign}(\omega) \, \mathrm{e}^{\mathrm{i}\omega l} \, \mathrm{d}\omega. \tag{B.2}$$

It is easy to see that $\mathbf{H}^2 = -\mathbf{I}$, here **I** is the identity operator. For any weighting function $w(l)$ with $c_1 \leqslant w(l) \leqslant c_2$, here c_1 and c_2 are positive constants, we have the relations:

$$T(w(l)l) = T(l)/w^2(l), \tag{B.3}$$

$$H(w(l)l) = H(l)/w(l). \tag{B.4}$$

Let $w(l) = \frac{K \sin l}{l}$, and using the Shepp–Logan filter, we have the following regularized expression of $T(K \sin l)$ when $-\pi/2 < l < \pi/2$,

$$\begin{aligned} T(K \sin l) &= T\left(\frac{K \sin l}{l} l\right) \\ &= \frac{l^2}{(K \sin l)^2} T(l) \\ &= \frac{l^2}{(K \sin l)^2} \frac{1}{2\pi} \int_{-\infty}^{\infty} |\omega| \, \mathrm{e}^{\mathrm{i}\omega l} \, \mathrm{d}\omega \\ &\approx \frac{l^2}{2\pi (K \sin l)^2} \int_{-\pi/\delta}^{\pi/\delta} |\omega| \frac{2 \sin(\delta\omega/2)}{\omega\delta} \, \mathrm{e}^{\mathrm{i}l\omega} \, \mathrm{d}\omega \\ &= \frac{l^2}{\pi (K \sin l)^2} \int_{-\pi/\delta}^{\pi/\delta} \frac{|\sin(\delta\omega/2)|}{\delta} \, \mathrm{e}^{\mathrm{i}l\omega} \, \mathrm{d}\omega \\ &= \frac{l^2}{(K \sin l)^2} \mathrm{SL}_\delta(l), \end{aligned} \tag{B.5}$$

where $\mathrm{SL}_\delta(l) = \frac{1}{\pi} \int_{-\pi/\delta}^{\pi/\delta} \frac{|\sin(\delta\omega/2)|}{\delta} \, \mathrm{e}^{\mathrm{i}l\omega} \, \mathrm{d}\omega$ is the Shepp–Logan filter, and its discrete version takes the following form,

$$\mathrm{SL}_\delta(n\delta) = 1.0/[\pi(0.25 - n^2)\delta^2]. \tag{B.6}$$

Therefore, equation (24) has been established.

Equation (32) is another variation of $T(l)$ based on the use of the ramp filter. In practice, $w(l)$ can be chosen according to the detector geometry or reconstruction factors such as the non-uniform sampling step and noise level. On the other hand, the weighting function $w(l)$ could use different cutoff frequencies for different values l so that a certain non-uniformity is included in the discretization of the exact reconstruction formula.

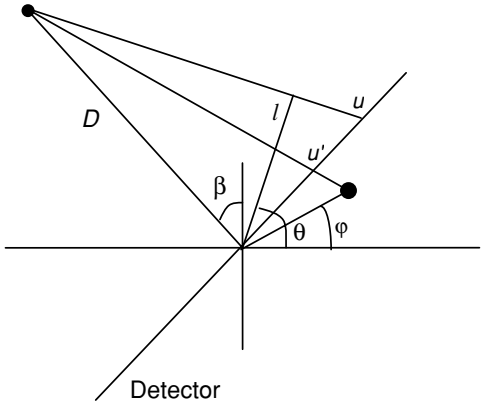

Figure 8. Equally spaced fan-beam collimator detector coordinate.

Appendix C. FBP algorithms for equally spaced collimators

An imaging geometry with an equally spaced fan-beam collimator detector is shown in figure 8, where the u-axis is parallel to the detector. The relation between the parallel-beam geometry and the fan-beam geometry is expressed as

$$l = \frac{uD}{\sqrt{D^2+u^2}} \qquad \text{and} \qquad \theta = \beta + \tan^{-1}\frac{u}{D}, \tag{C.1}$$

the Jacobian of the transformation from (u, β) to (l, θ) is $D^3/(D^2+u^2)^{3/2}$, which is always positive.

From [12], we have the following relation,

$$r\cos(\theta-\varphi) - l = K(u'-u), \tag{C.2}$$

where

$$K = \frac{D + r\sin(\beta-\varphi)}{\sqrt{D^2+u^2}}, \tag{C.3}$$

and

$$u' = \frac{Dr\cos(\beta-\varphi)}{D + r\sin(\beta-\varphi)}. \tag{C.4}$$

Let $k(u, \beta)$ represent the fan-beam projection of the same attenuation map $\mu(x, y)$ in the coordinate system (u, β), then the angular Hilbert transform $\mathbf{\Gamma}$ can be expressed as

$$[\mathbf{\Gamma}g](u) = \frac{\sqrt{u^2+D^2}}{\pi}\int_{-\infty}^{\infty}\frac{g(v)\,\mathrm{d}v}{(u-v)\sqrt{v^2+D^2}}. \tag{C.5}$$

Therefore the weighting function, i.e., the counterpart of (20), for the equally spaced fan-beam collimation geometry can be calculated as

$$\mathrm{e}^{h(l,\theta)}\big|_{l=\frac{uD}{\sqrt{D^2+u^2}},\theta=\tan^{-1}(\frac{u}{D})+\beta} = \mathrm{e}^{\frac{1}{2}[(\mathbf{I}+\mathrm{i}\mathbf{\Gamma})k](u,\beta)}. \tag{C.6}$$

Define $g(u, \beta)$ as

$$g(u,\beta) = \mathrm{e}^{\frac{1}{2}[(\mathbf{I}+\mathrm{i}\mathbf{\Gamma})k](u,\beta)}\,p\left(\frac{uD}{\sqrt{D^2+u^2}}, \beta + \tan^{-1}\frac{u}{D}\right). \tag{C.7}$$

Following similar calculations as for obtaining equation (23), define

$$U = (D + r\sin(\beta - \varphi))/D. \tag{C.8}$$

Then we are able to have the following FBP reconstruction formula in the coordinate system (u, β),

$$f(r,\varphi) = \frac{1}{4\pi}\,\mathrm{Re}\int_0^{2\pi}\frac{W_\beta(r,\varphi,u')}{U^2}\,\mathrm{d}\beta\int_{-\infty}^{\infty}T(u'-u)\frac{D}{\sqrt{u^2+D^2}}g(u,\beta)\,\mathrm{d}u + \frac{1}{4\pi}\,\mathrm{Re}\int_0^{2\pi}\frac{W_\beta^1(r,\varphi,u')}{U}\,\mathrm{d}\beta\int_{-\infty}^{\infty}H(u'-u)\frac{D^2}{u^2+D^2}g(u,\beta)\,\mathrm{d}u, \tag{C.9}$$

where

$$W_\beta(r,\varphi,u') = \mathrm{e}^{a_\theta(s,t)-h(s,\theta)}|_{\theta=\tan^{-1}(\frac{u'}{D})+\beta,s=r\cos(\theta-\varphi),t=r\sin(\theta-\varphi)} \tag{C.10}$$

and

$$W_\beta^1(r,\varphi,u') = \left.\frac{\partial \mathrm{e}^{a_\theta(s,t)-h(s,\theta)}}{\partial s}\right|_{\theta=\tan^{-1}(\frac{u'}{D})+\beta,s=r\cos(\theta-\varphi),t=r\sin(\theta-\varphi)}. \tag{C.11}$$

References

[1] Shepp L and Logan B 1974 The Fourier reconstruction of a head section *IEEE Trans. Nucl. Sci.* **21** 21–43

[2] Tretiak O and Metz C E 1980 The exponential Radon transform *SIAM J. Appl. Math.* **39** 341–54

[3] Novikov R G 2002 An inversion formula for the attenuated X-ray transformation *Ark. Math.* **40** 145–67

[4] Natterer F 2001 Inversion of the attenuated Radon transform *Inverse Problems* **17** 113–9

[5] Kunyansky L A 2001 A new SPECT reconstruction algorithm based on the Novikov explicit inversion formula *Inverse Problems* **17** 293–306

[6] You J 2005 Noise analysis and treatment for SPECT imaging via an FBP algorithm with classical filters *Technical Report* IRIS Lab., Dept of Radiology, State University of New York at Stony Brook

[7] Herman G T and Naparstek A V 1977 Fast image reconstruction based on a Radon inversion formula appropriate for rapidly collected data *SIAM J. Appl. Math.* **33** 511–33

[8] Horn B K P 1979 Fan-beam reconstruction methods *Proc. IEEE* **67** 1616–23

[9] You J, Liang Z and Zeng G L 1999 A unified reconstruction framework for both parallel-beam and variable focal-length fan-beam collimators by a Cormack-type inversion of exponential Radon transform *IEEE Trans. Med. Imaging* **18** 59–65

[10] Bukhgeim A A and Kazantsev S G 2002 Inversion formula for the fan-beam attenuated Radon transform in a unit disk *Preprint 99* The Sobolev Institute of Mathematics, Russian Academy of Science Siberian Branch

[11] Noo F, Defrise M, Clackdoyle R and Kudo H 2002 Image reconstruction from fan-beam projections on less than a short scan *Phys. Med. Biol.* **47** 2525–46

[12] Kak A C and Slaney M 1987 *Principles of Computerized Tomography* (Piscataway, NJ: IEEE)

[13] Press W H, Teukolsky S A, Vetterling W T and Flannery B P 1992 *Numerical Recipes in C* (Cambridge: Cambridge University Press)

[14] Guillement J P and Novikov R 2004 A noise property analysis of single-photon emission computed tomography data *Inverse Problems* **20** 175–98